ACS Macro Letters

pubs.acs.org/macroletters Letter

Impact of Entanglement on Folding of Semicrystalline Polymer during Crystallization

Fan Jin, Zheng Huang, Ying Zheng, Chenxuan Sun, Navin Kafle, Jiayang Ma, Pengju Pan, and Toshikazu Miyoshi*

Cite This: ACS Macro Lett. 2023, 12, 1138−1143 Read Online

ABSTRACT: Upon cooling, semicrystalline polymers experience crystallization and form alternatively stacked layers consisting of thin crystal lamellae and amorphous ones. The unique morphology, crystallinity, and crystallization kinetics highly depend on the molecular weight. Therefore, it is deduced that entanglement impacts crystallization kinetics, as well as hierarchically crystalline structures. However, the impact of entanglement on folded crystalline chains has not been well understood due to experimental difficulties. In this work, chain-folding structures for seven ^{13}C CH_3 labeled poly(L-lactic acid)s with various molecular weights (M_ws) were investigated by ^{13}C−^{13}C double quantum NMR spectroscopy. As a result, chain-folding events were categorized into three different M_w regimes: (i) The lowest M_w sample (2K g/mol) adopts an extended chain conformation (folding number, n = 0) (regime I); (ii) Intermediate M_w ones possess mixtures of non- and once-folded structures, and the once-folded fraction suddenly increases above the entanglement length (M_e), up to M_w = 45K g/mol (regime II); (iii) The high M_w ones (M_w > 45K g/mol) adopt the highest chance for an adjacent re-entry structure with n = 1.0 in the well-developed entangled network (regime III). It was suggested that entanglement induces folding of the semicrystalline polymer.

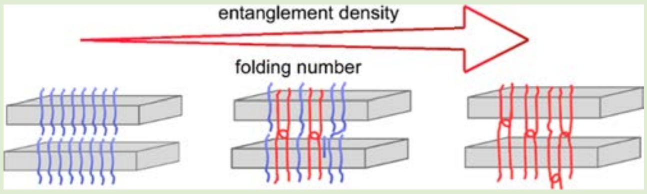

Two thirds of polymers are semicrystalline.[1−5] Excellent thermal and mechanical properties of various semicrystalline polymers play important roles in our lives. One good example is polyethylene, which is widely used in our lives from convenient plastic bags to bullet proof materials. Many researchers have focused on understanding crystallization mechanisms as well as the crystalline structures of semicrystalline polymers in the past decades. Upon cooling, semicrystalline polymers form isolated single crystals in a dilute solution and form alternatively stacked layers from a melt.[2] The radius of gyration (R_g) in the single crystal is much smaller than that for the melt-grown crystal.[5−7] Furthermore, viscosity of polymer melts[8] as well as crystallinity,[9] crystal−crystal transition,[10] morphology,[2−4] and toughness/brittleness[11] of semicrystalline polymers highly depend on molecular weight (M). The accumulated results imply that crystallization and crystalline structures are significantly influenced by entanglement.[4] Various theories have been developed to understand polymer crystallization at the molecular level.[12−15] Among them, the well-known secondary nucleation theory[12,13] deduced the molecular events of long polymer chains on the growth surface as follows: Polymers are dragged into the existing crystal surface and experience partial disentanglements; the disentangled chains fold on the growth front, and the single chain process via folding (intramolecular event) competes with other chains (intermolecular one). Therefore, it is believed that intrachain and interchain crystallization processes highly depend on kinetics.[12,13] However, understanding the folding structure itself has been a debatable matter in the past decades.[16−19] Therefore, it is not understood how entanglement impacts the folding structure of a long polymer chain during crystallization.

Recent progress of computation methods/power[20−24] as well as experimental tools[25−29] could allow one to evaluate the chain-folding structure of semicrystalline polymers. It was indicated that (i) flexible polymer chains adopt a long-range order of adjacent re-entry structure in the solution-grown crystals[27,30−35] and monolayer films,[25,36,37] whereas the mean number for adjacent re-entry structure, n, is limited to a few times in the melt-grown crystals.[31,38,39] Among several advanced techniques, ^{13}C−^{13}C double quantum (DQ)[29,40] NMR spectroscopy combined with ^{13}C selective isotope labeling enabled one to study the chain-folding structure in wide supercooling (ΔTs). It was demonstrated that experimentally available kinetics does not change the folding number of *isotactic*-poly(1-butene),[31] *isotactic*-polypropylene,[38] and poly(L-lactic acid) (PLLA)[39] in the melt-grown crystals. Furthermore, Jin et al. studied the chain-folding structure of

Received: June 14, 2023
Accepted: July 25, 2023
Published: July 28, 2023

PLLA in an extreme case, so-called, a rapidly quenched glass. It was found that polymer chains fold prior to crystallization.[41] Luo and Sommer, using a coarse-grained (CG) poly(vinyl alcohol) (PVA) model,[20−22] reported that (i) the entanglement length (M_e) decreases due to chain stiffening during cooling and increases due to partial disentanglements during crystallization,[20] (ii) PVA-CG chains adjacently fold and the adjacent re-entry number (n = 1.0−1.2) is invariant as a function of crystallization temperature (T_c),[21] (iii) lamellae thickness (L) and folding number, n, are directly related to M_e.[21] The recent results inferred the important role of entanglement in polymer crystallization at the molecular levels. To further understand polymer crystallization, M dependence of the folding structure, especially across M_e and the critical entanglement length (M_c), is necessary.

In this work we investigate the chain-folding structure for seven ^{13}C CH_3-labeled (l) PLLAs with various weight-average molecular weights (M_ws) across M_e = 7.7−8.0K g/mol and M_c[42,43] by using ^{13}C−^{13}C DQ NMR spectroscopy. Seven l-PLLA samples with M_w = 2K−300K g/mol were successfully synthesized by using two recycling routes of l-polymers and l-intermediate compounds (see details in the Supporting Information (SI) and Figure S2). To study the chain-folding structure, l-PLLA was diluted by 90% with nonlabeled (n)-PLLAs with similar M_ws. The M_w and PDI of l- and n-PLLAs are listed in Table 1. A small supercooling, ΔT = melting temperature (T_m) − T_c of 25−30 °C, was used for isothermal crystallization to minimize a potential kinetics effect. Crystallization conditions are provided in the SI.

Table 1. M_w, PDI, Chain Length (L_{ECC}) under the Assumption of a Fully Extended 10_3 Helix, and a Mean Number for Successive Adjacent Re-Entry Structure (n) of l-PLLAs and L_0 of l-/Nonlabeled (n-) PLLA Blends Used in This Work[a]

sample name	M_w[b] (K g/mol)	PDI	L_0 (nm)	L_{ECC} (nm)	n
l-2k (n-2k)	2.0 (2.3)	1.24 (1.26)	7.9	7.8	0
l-4k (n-5k)	4.4 (4.8)	1.54 (1.35)	13.2	16.9	0.2
l-9k (n-10k)	8.7 (10.0)	1.78 (1.62)	16.0	34.0	0.6
l-24k (n-20k)	24.3 (20.4)	2.00 (1.53)	18.1	94.5	0.7
l-45k (n-44k)	45.0 (43.6)	1.45 (1.66)	24.0	175	0.9
l-74k (n-71k)	73.5 (71.1)	1.54 (1.90)	26.0	286	1.0
l-300k (n-248k)	300 (248)	2.26 (2.28)	28.3	1167	1.0

[a]The inside bracket represents the corresponding values for n-PLLA. [b]M_w was corrected by a factor of 0.58 by using polystyrene as the standard.

Figure 1a depicts the first heating DSC profiles for seven l-/n-PLLA blends after the isothermal crystallization. The l-2k blend shows broad and complex melting peaks at 120−140 °C. l-4k depicts doublet T_m peaks at 152 and 156 °C. A higher M_w than l-9K g/mol leads to a singlet T_m peak, which shifts to a higher temperature with increasing M_w. It is understood that the melting behaviors for the low M_w samples are influenced by PDI. Figure 1c shows small-angle X-ray scattering (SAXS) patterns for seven l-/n-PLLA blends. Long periods (L_0) are listed in Table 1. L_0 increases with increasing M_w, as similarly observed in T_m. As opposed to M_w dependences of T_m and L_0, the polarized optical microscope (POM) image shows a unique M_w dependence of morphology. Small M_w samples of the l-2k and l-4k blends show needlelike morphology (Figures 1b and S3). The image for the l-9k blend shows a mixture of needles and spherulites. The relative ratio of the former and latter is almost 1:1. Therefore, coexistence of two types of morphology is not attributed to isotope effect but to PDI. Larger M_w samples > l-9K g/mol show only spherulites. These morphological transitions may be related to entanglement (M_e = 7.7[42]−8.0 K[43] g/mol). Figure 1d provides a ^{13}C cross-polarization (CP) magic angle spinning (MAS) NMR spectrum for l-24k/n-20k blends with a mixing ratio of 1:9 measured at ambient temperature. Detailed NMR experimental conditions are given in SI. ^{13}C CH_3 signals give ∼3.8-fold higher peak area than the CH and CO signals due to the ^{13}C isotope effect. The same intensity ratio of CH_3 to CH carbon guarantees the same blending ratio in seven blends (Figure S4). All CH_3, CH, and CO groups show fine splitting with numbers of 2, 4, and 5, respectively.[44,45] These peaks correspond to inequivalent conformation sites in 10_3 helix in the thermodynamically stable α crystal.[46] Sharp and broad Lorentzian peaks corresponding to the crystalline and amorphous signals, respectively, were applied to either the CO or CH peak. Crystallinity for the l-24k blend is determined to be 84%. It was found that crystallinity decreases to 74% with increasing M_w (Figure S4).

The packing structure of seven l-PLLAs were investigated by using ^{13}C−^{13}C DQ NMR spectroscopy (see details in the Experimental Section in the SI).[41] Figure 2a,b shows ^{13}C−^{13}C DQ buildup curves for l-4k (pink circle), 9k (blue), and 24k (cyan), and 45k (green), 74k (orange), and 300k (red), respectively. All six buildup curves are very consistent with each other. Statistical spin-dynamics simulation[47] was conducted based on the atomic coordinates of the CH_3 group for PLLA α crystal determined by using fiber X-ray diffraction (closest stem−stem (SS) distance is 6.1 Å),[46] where all statistical dipolar interactions with a distance within 7 Å were took into consideration (see refs 29, 33, and 41). One of the possible spin systems including a reference (red) and 13 surrounding spins (blue) is schematically depicted in Figure 2a. In addition, DQ buildup curves were further simulated under the assumption of SS distance of 5.9 and 6.3 Å. The simulated curves with SS distance of 5.9 (dotted black), 6.1 (solid), and 6.3 Å (dashed) with a relaxation parameter of T_2 = 9.8 ms were plotted in Figure 2a and with the distance of 6.1 Å (solid red) in Figure 2b. By comparison of the experimental curve with the simulated ones, it is concluded that six l-4k−300k samples adopt the same SS distance of 6.1 Å in the crystalline region.[46] ^{13}C−^{13}C DQ buildup curve for l-2k (open black circle) was slightly faster and peak maximum height was lower than those of others, was plot in Figure 2b. The experimental curve was reproduced by using SS = 5.9 Å and T_2 = 8.4 ms (black solid curve). The atomic coordinates of ^{13}C-labeled nuclear spins and the T_2 values used for the packing analysis were further used for the chain-folding analysis of seven l-/n-PLLA blends.

In the l-/n-PLLA blends with a mixing ratio of 1:9, dipolar interactions dominantly originate from intramolecular interactions of the l-PLLA chain diluted in the n-PLLA matrix. Figure 3a schematically illustrates one example of ^{13}C spin distribution of the l-PLLA chain, where ^{13}C stems connected via folding with n = 0, 1, and 2 being highlighted by pink circles. Folding generates intrachain dipolar interactions and thus increases the DQ curve's height depending on n (Figure 3a). Note that minor effects of statistical ^{13}C-labeled

https://doi.org/10.1021/acsmacrolett.3c00364
ACS Macro Lett. 2023, 12, 1138−1143

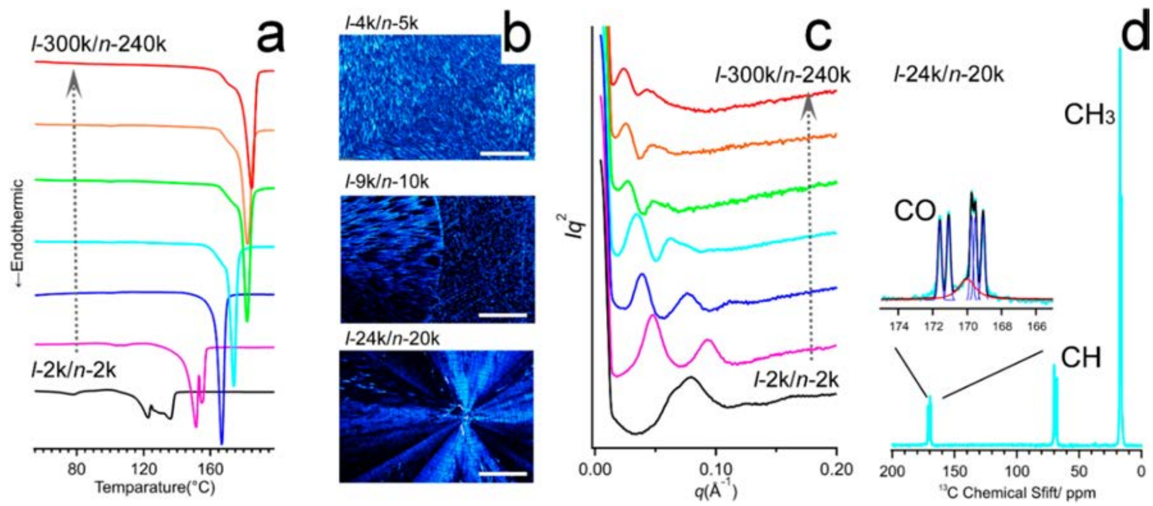

Figure 1. (a) DSC heating curves with a heating rate of 10 °C/min and (c) SAXS patterns of *l*-/*n*-PLLA blends as a function of M_w. (b) POM images for the *l*-4k/*n*-5k (top), *l*-9k/*n*-10k (middle), and *l*-24k/*n*-20k blends (bottom). The white scale bar represents 500 μm. (d) ^{13}C CPMAS NMR spectrum for the *l*-24k/*n*-20k blend, respectively, at the MAS frequency of 10k ± 5 Hz. The expanded spectrum for the CO group with the best-fitted peaks.

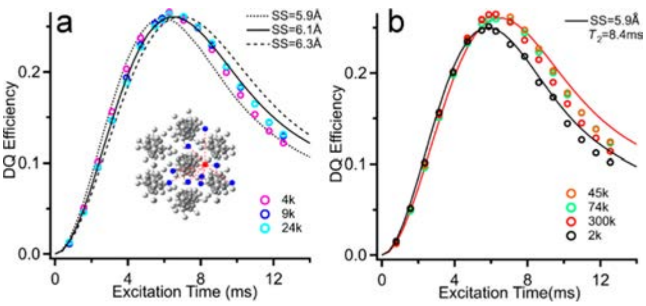

Figure 2. Experimental DQ buildup curves (open circle) for (a) *l*-4k (pink), *l*-9k (blue), and *l*-24k (cyan) and (b) *l*-45k (green), *l*-74k (orange), *l*-300k (red), and *l*-2k (black), with simulated DQ buildup curves with (a) T_2 = 9.8 ms and SS = 5.9 Å (dotted black curve), 6.1 Å (solid) and 6.3 Å (dashed), and with (b) SS = 6.1 Å and T_2 = 9.8 ms (solid red), and SS = 5.9 Å and T_2 = 8.4 ms (solid black).

interchain[29] and natural abundance of ^{13}C CH_3 carbon[41] were taken into consideration.

Figure 3b−d depicts DQ buildup curves for *l*-/*n*-PLLA blends as a function of M_w. It is found that the DQ curve height increases with increasing M_w up to 74K g/mol and is finally saturated in the high M_w range. Depending on the experimental results, different three regimes could be identified as follows: In regime I, the DQ curve for *l*-2k in the blend was fitted with $n = 0$. Namely, the lowest M_w sample forms ECC. Besides, the ECC structure is supported by L_0 = 7.9 nm, which is like L_{ECC} = 7.8 nm under the assumption of 10_3 helical conformation. In $M_w \geq$ 4000 g/mol, L_{ECC} is longer than L_0 (Table 1). L_0 no longer gives information about the chain-level structure. In regime II (M_w = 4K−45K g/mol), the n value for *l*-4k was determined to be 0.2 (Figure 3c). This structure can be represented in terms of mixture of non- and once-folded structure, and the former is dominant. With increasing M_w slightly larger than M_e,[42,43] the n value jumped up to 0.6 for *l*-9k (Figure 3c). Further increasing M_w increased n to 0.7 for *l*-24k (Figure S5) and 0.9 for *l*-45k (Figure 3c). These findings indicate that intermolecular packing is gradually replaced by intramolecular packing via folding above M_e in regime II. There is a positive correlation between the entanglement density and folding number. In regime III ($M_w \geq$ 74 k g/mol), DQ curve height reached a maximum and was independent of M_w, as demonstrated in Figure 3d. The best-fitting curve to the experimental one gave n = 1.0, where the chance for intramolecular packing is the highest among seven samples and equal to that for intermolecular packing. Note that the n value of 1.0 in regime III is slightly lower than the previously reported n value of 1.5−2.0 in PLLA with different M_ws.[39] Current simulation includes the natural abundance effect of ^{13}C CH_3 carbon and thus accurately determines the n value.[41]

According to the secondary nucleation theory,[12,13] polymer chains are dragged into the growth front and are partially disentangled and fold on the growth front. The degree of disentanglement would depend on chain mobility as well as the entanglement number. To minimize the difference in chain mobility, ΔT was set to 25−30 °C. The *l*-9k and *l*-24k samples have smaller entanglement numbers of 1 and 2, respectively, prior to crystallization than the *l*-300k sample (ca. 38). Considering L_0 and L_{ECC}, it was expected that *l*-9k and 24k samples ideally fold more than 1 and 2 times, respectively. However, the former and latter fold only 0.6 and 0.7 times, which are lower than the expectation as well as n = 1.0 for the higher M_w ones. This fact means that even though disentanglement partially occurs in the intermediate M_w samples, the disentangled chains do not prefer folding and rather form intermolecular packing. The intermolecular packing is simply explained in terms of the high concentration of the PLLA chains in the highly condensed melt. Another important finding is that hairpin structure (intramolecular packing) is formed only in the well-developed entangled networks. The unique M_w dependence of folding can be naturally explained in terms of induction by entanglements. Namely, entanglement has a positive impact on the folding of semicrystalline polymers; however, it limits adjacent re-entry number (n = 1.0) during crystallization. This mechanism explains our recent observation that a rapidly quenched PLLA glass adopts the same hairpin structure with the α crystals.[41] Traditionally, it has been believed that chain-folding structure is located at the crystal−amorphous interface in the polymer crystals.[12,13] However, there is no experimental evidence to

https://doi.org/10.1021/acsmacrolett.3c00364
ACS Macro Lett. 2023, 12, 1138−1143

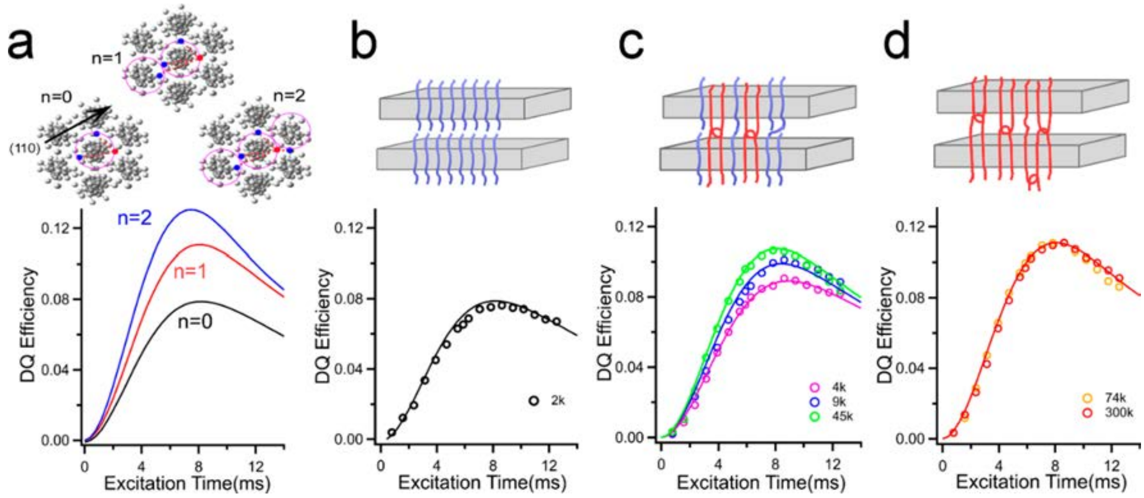

Figure 3. (a) Schematic illustrations of the chain-folding structure of *l*-PLLA with n = 1 and 2 along the crystallographic (110) direction and corresponding DQ simulations curves with SS = 6.1 Å and T_2 = 9.8 ms, and ECC structure with n = 0 and corresponding simulation curve with SS = 5.9 Å and T_2 = 8.4 ms (black curve). ^{13}C-labeled stems are illustrated by pink circles and ^{13}C atoms are highlighted by red (reference one) and blue circles (surrounding ones). Experimental DQ buildup curves of (b) *l*-2k (black open circle), (c) *l*-4k (pink), *l*-9k (blue), *l*-45k (green), and (d) *l*-74k (orange), and *l*-300k (red) blends and best-fit simulation curves to *l*-2k, *l*-4k, *l*-9k, and *l*-300k blends with n = 0 (black solid curve), 0.2 (pink), 0.6 (blue), 0.9 (green), and 1.0 (red). Schematic illustrations for (b) ECC (n = 0), (c) mixture of non- and once-folded structure, and (d) once-folded structure (n = 1.0).

support a tight fold in the melt-grown crystals. The newly established relationship between folding and entanglement revises not only the folding mechanism, but also the locations and roles of folding in the met-grown crystals. Our finding suggests the following scenario in polymer crystallization. Initially, entanglement of two chains naturally generates a loose fold loop in the melt state. Subsequent cooling induces chain stiffing and decreases M_e. This process results in tight folding.[20] Afterwords, nucleation and growth induce conformational and packing ordering accompanying partial disentanglements, but they still preserve the topological constraints. Crystallization pushes out some folding structures, as well as entanglements from the crystalline region. As results, some may be located at the crystal−amorphous interface but others in the amorphous region (Figure 3c,d). Therefore, the folding structure liked with entanglement might play a vital role for morphological development,[2−4] selections of lamellar thickness,[48,49] crystal−crystal transition,[10] deformation and mechanical property,[11,50] etc., of semicrystalline polymers.

■ ASSOCIATED CONTENT

Supporting Information

The Supporting Information is available free of charge at https://pubs.acs.org/doi/10.1021/acsmacrolett.3c00364.

> Synthesis and recycling protocol, experimental conditions, ^{1}H solution-state NMR spectrum of ^{13}C 33% labeled (*l*) lactide, ^{13}C CPMAS spectra for *l*-PLLAs and their blends, POM images for *l*-2k, *l*-45k, *l*-74k, and *l*-300k blends and DQ buildup curves for *l*-24k and *l*-74k blends and simulation curves (PDF)

■ AUTHOR INFORMATION

Corresponding Author

Toshikazu Miyoshi − *School of Polymer Science and Polymer Engineering, The University of Akron, Akron, Ohio 44325-3909, United States;* orcid.org/0000-0001-8344-9687; Email: miyoshi@uakron.edu

Authors

Fan Jin − *School of Polymer Science and Polymer Engineering, The University of Akron, Akron, Ohio 44325-3909, United States*

Zheng Huang − *School of Polymer Science and Polymer Engineering, The University of Akron, Akron, Ohio 44325-3909, United States;* orcid.org/0000-0001-5268-1272

Ying Zheng − *School of Polymer Science and Polymer Engineering, The University of Akron, Akron, Ohio 44325-3909, United States; State Key Laboratory of Chemical Engineering, College of Chemical and Biological Engineering, Zhejiang University, Hangzhou 310027, China; Institute of Zhejiang University-Quzhou, Quzhou 324000, China;* orcid.org/0000-0002-2379-6342

Chenxuan Sun − *School of Polymer Science and Polymer Engineering, The University of Akron, Akron, Ohio 44325-3909, United States; State Key Laboratory of Chemical Engineering, College of Chemical and Biological Engineering, Zhejiang University, Hangzhou 310027, China; Institute of Zhejiang University-Quzhou, Quzhou 324000, China;* orcid.org/0000-0001-8108-3255

Navin Kafle − *School of Polymer Science and Polymer Engineering, The University of Akron, Akron, Ohio 44325-3909, United States*

Jiayang Ma − *School of Polymer Science and Polymer Engineering, The University of Akron, Akron, Ohio 44325-3909, United States*

Pengju Pan − *State Key Laboratory of Chemical Engineering, College of Chemical and Biological Engineering, Zhejiang University, Hangzhou 310027, China; Institute of Zhejiang University-Quzhou, Quzhou 324000, China;* orcid.org/0000-0001-6924-5485

Complete contact information is available at: https://pubs.acs.org/10.1021/acsmacrolett.3c00364

Author Contributions

F.J. and C.S. synthesized samples. F.J and Z.H. conducted DQ buildup curve simulations. P.P. and T.M. conceived and designed experiments. F.J., Z.H., Y.Z., J.M., and N.K. conducted NMR, SAXS, POM, and DSC experiments. The manuscript was written through contributions of all authors. All authors have given approval to the final version of the manuscript. CRediT: **Fan Jin** data curation (lead), formal analysis (lead), investigation (lead), methodology (lead), resources (lead), software (lead), writing-original draft (lead), writing-review & editing (supporting); **Zheng Huang** formal analysis (equal), investigation (equal), methodology (equal), writing-original draft (supporting), writing-review & editing (supporting); **Ying Zheng** data curation (equal), formal analysis (equal), writing-original draft (supporting), writing-review & editing (supporting); **Navin Kafle** formal analysis (supporting), supervision (supporting), writing-original draft (supporting), writing-review & editing (supporting); **Jiayang Ma** formal analysis (supporting), writing-original draft (supporting), writing-review & editing (supporting); **Pengju Pan** conceptualization (supporting), supervision (equal), writing-original draft (supporting), writing-review & editing (supporting); **Toshikazu Miyoshi** conceptualization (lead), data curation (lead), formal analysis (lead), funding acquisition (lead), investigation (equal), methodology (lead), project administration (lead), resources (lead), software (lead), supervision (lead), validation (lead), visualization (lead), writing-original draft (lead), writing-review & editing (lead).

Notes

The authors declare no competing financial interest.

■ ACKNOWLEDGMENTS

This work was financially supported by NSF DMR Polymers 2004393.

■ REFERENCES

(1) Corradini, P.; Auriemma, F.; De Rosa, C. Crystals and Crystallinity in Polymeric Materials. *Acc. Chem. Res.* **2006**, *39*, 314−323.
(2) Lotz, B.; Miyoshi, T.; Cheng, S. Z. D. 50th Anniversary Perspective: Polymer Crystals and Crystallization: Personal Journeys in a Challenging Research Field. *Macromolecules* **2017**, *50*, 5995−6025.
(3) Tang, X.; Chen, W.; Li, L. The Tough Journey of Polymer Crystallization: Battling with Chain Flexibility and Connectivity. *Macromolecules* **2019**, *52*, 3575−3591.
(4) Seguela, R. Critical Review of the Molecular Topology of Semicrystalline Polymers: The Origin and Assessment of Intermolecular Tie Molecules and Chain Entanglements. *J. Polym. Sci., Part B: Polym. Phys.* **2005**, *43*, 1729−1748.
(5) Sadler, D. M.; Keller, A. Neutron Scattering Studies on the Molecular Trajectory in Polyethylene Crystallized from Solution and Melt. *Macromolecules* **1977**, *10*, 1128−1140.
(6) Fischer, E. W. Studies of structure and dynamics of solid polymers by elastic and inelastic neutron scattering. *Pure Appl. Chem.* **1978**, *50* (11−12), 1319−1341.
(7) Sadler, D. M.; Keller, A. Neutron Scattering of Solution-Grown Polymer Crystals: Molecular Dimensions Are Insensitive to Molecular Weight. *Science* **1979**, *203*, 263−264.
(8) Dealy, J. M.; Read, D. J.; Larson, R. G. *Structure and Rheology of Molten Polymers*, 2nd ed.; Hanser Publications, 2018.
(9) Mandelkern, L. *Acc. Chem. Res.* **1990**, *23*, 380−386.
(10) Qiao, Y.; Yang, F.; Lu, Y.; Liu, P.; Li, Y.; Men, Y. Crystallization Temperature Reveals Stabilization Role of Intercrystalline Links and Entanglements for Metastable Form II Crystals. *Macromolecules* **2018**, *51*, 8298−8305.
(11) Cho, S. H.; Register, R. A. Minimum Molecular Weight and Tie Molecules Content for Ductility in Polyethylene of Varying Crystallinity. *Macromolecules* **2022**, *55*, 3249−3258.
(12) Lauritzen, J. I.; Hoffman, J. D. Theory of Formation of Polymer Crystals with Folded Chains in Dilute Solution. *J. Res. Natl. Bur. Stand., Sect. A* **1960**, *64A*, 73.
(13) Hoffman, J. D.; Miller, R. L. Kinetic of Crystallization from the Melt and Chain Folding in Polyethylene Fractions Revisited: Theory and Experiment. *Polymer* **1997**, *38*, 3151−3212.
(14) Strobl, G. From the Melt via Mesomorphic and Granular Crystalline Layers to Lamellar Crystallites: A Major Route Followed in Polymer Crystallization? *Eur. Phys. J. E: Soft Matter Biol. Phys.* **2000**, *3*, 165−183.
(15) Allegra, G.; Meille, S. V. Pre-Crystalline, High-Entropy Aggregates: A Role in Polymer Crystallization? *Adv. Polym. Sci.* **2005**, *191*, 87−135.
(16) Flory, P. J.; Yoon, D. Y. Molecular morphology in semicrystalline polymers. *Nature* **1978**, *272*, 226−229.
(17) Guttman, C. M.; DiMarzio, E. A.; Hoffman, J. D. Calculation of SANS Intensity for Polyethylene: Effect of Varying Fold Planes and Fold Plane Roughening. *Polymer* **1981**, *22*, 597−608.
(18) Jing, X.; Krimm, S. Mixed-Crystal Infrared Studies of Chain Folding in Melt-Crystallized Polyethylene. *J. Polym. Sci., Polym. Lett. Ed.* **1983**, *21*, 123−130.
(19) Sadler, D. M.; Harris, R. A Neutron Scattering Analysis: How Does the Conformation in Polyethylene Crystals Reflect That in the Melt? *J. Polym. Sci., Polym. Phys. Ed.* **1982**, *20*, 561−578.
(20) Luo, C.; Sommer, J. U. Disentanglement of Linear Polymer Chains Toward Unentangled Crystals. *ACS Macro Lett.* **2013**, *2*, 31−34.
(21) Luo, C.; Sommer, J. U. Role of thermal history and entanglement related thickness selection in polymer crystallization. *ACS Macro Lett.* **2016**, *5*, 30−34.
(22) Luo, C.; Kroger, M.; Sommer, J.-U. Entanglements and crystallization of concentrated polymer solutions: molecular dynamics simulations. *Macromolecules* **2016**, *49*, 9017−9025.
(23) Yamamoto, T. Molecular Dynamics of Crystallization in a Helical Polymer Isotactic Polypropylene from the Oriented Amorphous State. *Macromolecules* **2014**, *47*, 3192−3202.
(24) Yi, P. C.; Locker, R.; Rutledge, G. C. Molecular Dynamics Simulation of Homogeneous Crystal Nucleation in Polyethylene. *Macromolecules* **2013**, *46*, 4723−4733.
(25) Kumaki, J.; Kawauchi, T.; Yashima, E. Two-Dimensional Folded Chain Crystals of a Synthetic Polymer in a Langmuir-Blodget Film. *J. AM. Chem. Soc.* **2005**, *127*, 5788−5789.
(26) Savage, R. C.; Mullin, N.; Hobbs, J. K. Molecular Conformation at the Crystal-Amorphous Interphase in Polyethylene. *Macromolecules* **2015**, *48*, 6160−6165.
(27) Ma, Z.; Yang, P.; Zhang, X.; Jiang, K.; Song, Y.; Zhang, W. Quantifying the Chain Folding in Polymer Single Crystals by Single-Molecule Force Spectroscopy. *ACS Macro Lett.* **2019**, *8*, 1194−1199.
(28) Zeng, X.; Ungar, G.; Spells, S.; King, S. M. Real-Time Neutron Scattering Study of Transient Phases in Polymer Crystallization. *Macromolecules* **2005**, *38*, 7201−7204.
(29) Hong, Y-l.; Miyoshi, T. Chain-Folding Structure of a Semicrystalline Polymer in Bulk Crystals Determined by $^{13}C-^{13}C$ Double Quantum NMR. *ACS Macro Lett.* **2013**, *2*, 501−505.
(30) Hong, Y-l.; Miyoshi, T. Elucidation of the Chain-Folding Structures of a Semi-crystalline Polymer in Single Crystals by Solid-state NMR Spectroscopy. *ACS Macro Lett.* **2014**, *3*, 556−559.
(31) Hong, Y-l.; Koga, T.; Miyoshi, T. Chain Trajectory and Crystallization Mechanism of a Semicrystalline Polymer in Melt- and Solution-Grown Crystals As Studied Using $^{13}C-^{13}C$ Double-Quantum NMR. *Macromolecules* **2015**, *48*, 3282−3293.
(32) Hong, Y-l; Yuan, S.; Li, Z.; Ke, Y.; Nozaki, K.; Miyoshi, T. Three-Dimensional Conformation of Folded Polymers in Single Crystals. *Phys. Rev. Lett.* **2015**, *115*, 1−5.
(33) Wang, S.; Yuan, S.; Chen, W.; He, Q.; Hong, Y-l.; Miyoshi, T. Solid-State NMR Study of the Chain Trajectory and Crystallization

Mechanism of Poly(L-Lactic Acid) in Dilute Solution. *Macromolecules* **2017**, *50*, 6404−6414.
(34) Wang, S.; Yuan, S.; Chen, W.; Zhou, Y.; Hong, Y-l.; Miyoshi, T. Structural Unit of Polymer Crystallization in Dilute Solution As Studied by Solid-State NMR and ^{13}C Isotope Labeling. *Macromolecules* **2018**, *51*, 8729−8737.
(35) Hong, Y-l.; Chen, W.; Yuan, S.; Kang, J.; Miyoshi, T. Chain Trajectory of Semicrystalline Polymers As Revealed by Solid-State NMR Spectroscopy. *ACS Macro Lett.* **2016**, *5*, 355−358.
(36) Anzai, T.; Kawauchi, M.; Kawauchi, T.; Kumaki, J. Crystallization Behavior of Single Isotactic Poly(methyl methacrylate) Chains Visualized by Atomic Force Microscopy. *J. Phys. Chem. B* **2015**, *119*, 338−347.
(37) Ono, Y.; Kumaki, J. In Situ Real-Time Observation of Polymer Folded-Chain Crystallization by Atomic Force Microscopy at The Molecular Level. *Macromolecules* **2018**, *51*, 7629−7636.
(38) Yuan, S.; Li, Z.; Hong, Y.-l.; Ke, Y.; Kang, J.; Kamimura, A.; Otsubo, A.; Miyoshi, T. Folding of Polymer Chains in the Early Stage of Crystallization. *ACS Macro Lett.* **2015**, *4*, 1382−1385.
(39) Wang, S.; Yuan, S.; Wang, K.; Chen, W.; Yamada, K.; Barkley, D.; Koga, T.; Hong, Y.-l.; Miyoshi, T. Intramolecular and Intermolecular Packing in Polymer Crystallization. *Macromolecules* **2019**, *52*, 4739−4748.
(40) Hohwy, M.; Jakobsen, H. J.; Edén, M.; Levitt, M. H.; Nielsen, N. C. Broadband Dipolar Recoupling in the Nuclear Magnetic Resonance of Rotating Solids: A Compensated C7 Pulse Sequence. *J. Chem. Phys.* **1998**, *108*, 2686−2694.
(41) Jin, F.; Yuan, S.; Wang, S.; Zheng, Y.; Zhang, Y.; Hong, Y. L.; Miyoshi, T. Polymer Chains Fold Prior to Crystallization. *ACS Macro. Lett.* **2022**, *11*, 284−288.
(42) Ren, J.; Urakawa, O.; Adachi, K. Dielectric and Viscoelastic Studies of Segmental and Normal Mode Relaxations in Undiluted Poly(d, l-lactic acid). *Macromolecules* **2003**, *36*, 210−219.
(43) Cooper-White, J. J.; Mackay, M. E. Rheological Properties of Poly(lactide). Effect of Molecular Weight and Temperature on the Viscoelasticity of Poly(L-Lactic Acid). *J. Polym. Sci. Part B, Polym. Phys.* **1999**, *37*, 1803−1814.
(44) Chen, W.; Reichert, D.; Miyoshi, T. Short-Range Correlation of Successive Helical Jump Motions of Poly(L-Lactic Acid) Chains in the α Phase as Revealed by Solid-State NMR. *J. Phys. Chem. B* **2015**, *119*, 4552−4563.
(45) Chen, W.; Zhou, W.; Makita, Y.; Wang, S.; Yuan, S.; Konishi, T.; Miyoshi, T. Characterization of the Slow Molecular Dynamics of Poly(l-Lactic Acid) in α and α' Phases, in a Glassy State, and in a Complex with Poly(d-Lactic Acid) by Solid-State NMR. *Macromol. Chem. Phys.* **2018**, *219*, No. 1700451.
(46) Sasaki, S.; Asakura, T. Helix Distortion and Crystal Structure of the α-Form of Poly (L -Lactide). *Macromolecules* **2003**, *36*, 8385−8390.
(47) Veshtort, M.; Griffin, R. G. SPINEVOLUTION: A Powerful Tool for the Simulation of Solid and Liquid State NMR Experiments. *J. Magn. Reson.* **2006**, *178*, 248−282.
(48) Kawai, T.; Rahman, N.; Matsuba, G.; Nishida, K.; Kanaya, T.; Nakano, M.; Okamoto, H.; Kawada, J.; Usuki, A.; Honma, N.; Nakajima, K.; Matsuda, M. Crystallization and Melting Behavior of Poly(L-lactic acid). *Macromolecules* **2007**, *40*, 9463−9469.
(49) Fujita, M.; Sawayanagi, T.; Abe, H.; Tanaka, T.; Iwata, T.; Ito, K.; Fujisawa, T.; Maeda, M. Stereocomplex Formation through Reorganization of Poly(L-Lactic Acid) and Poly(D-Lactic acid) Crystals. *Macromolecules* **2008**, *41*, 2852−2858.
(50) Romano, D.; Tops, N.; Bos, J.; Rastogi, S. Correlation between Thermal and Mechanical Response of Nascent Semicrystalline UHMWPEs. *Macromolecules* **2017**, *50*, 2033−2042.

https://doi.org/10.1021/acsmacrolett.3c00364
ACS Macro Lett. 2023, 12, 1138−1143